Journal of Power Sources 198 (2012) 143–148

Contents lists available at SciVerse ScienceDirect

Journal of Power Sources

journal homepage: www.elsevier.com/locate/jpowsour

Investigation of polymer electrolyte membrane fuel cell parallel flow field with induced cross flow

John Bachman, Anthony Santamaria, Hong-Yue Tang, Jae Wan Park*

Department of Mechanical and Aerospace Engineering, University of California, Davis, CA 95616, United States

ARTICLE INFO

Article history:
Received 18 August 2011
Received in revised form
15 September 2011
Accepted 16 September 2011
Available online 21 September 2011

Keywords:
PEM fuel cell
Cross flow
Back pressure
Parallel flow field

ABSTRACT

We present a novel idea to utilize a parallel channel design with a pressure difference between channels in an effort to maintain a short flow path, while attaining the cross flow inherent in serpentine flow fields. For this study, a polymer electrolyte membrane (PEM) fuel cell with the ability to control the back pressure on every other flow channel (high pressure channels, HPCs), in order to induce cross flow from the high pressure to the low pressure channels (LPCs), was designed and built. Polarization curves for different back pressures on the HPCs and for different stoichiometries on the cathode were measured. Performance gains were found at the end of the ohmic and mass transport loss regimes (voltages under 0.55 V). Secondly, the current density and net power (subtracting approximate pumping work) were determined based on HPC back pressure at steady state voltages of 0.5 V, 0.3 V, and 0.1 V. The parallel flow field with induced cross flow at the optimal back pressure had up to a 24% improvement in current density and a 14% improvement in net power over the standard parallel channel design.

1. Introduction

Polymer electrolyte membrane (PEM) fuel cells, while needing moisture in the membrane, should minimize liquid water accumulation in the gas diffusion layer (GDL) and catalyst layer (CL). This balance must be maintained over varying operating conditions. Additionally, water migration is inhibited because it is created in the CL and must travel through the GDL into the channels in order to exit the cell. The GDL is a porous media in order to maintain electrical contact while allowing a path for reactants to reach the CL, however this can hinder water removal. Parallel channels are a common flow-field configuration that are used in most modern PEM fuel cell stack designs. Removing liquid water from the CL and GDL to the parallel flow channels is complex, as the water must travel transversely to the reactant flow. Such water transport may be driven by two main mechanisms in PEM fuel cells with parallel flow channels: the capillary force from the hydrophobicity of the GDL and the static pressure gradient created by the reactant flow speed in the flow channel. However, with parallel flow channels the reactant flow speed is low and may cause local flooding, particularly under lands, where the pressure gradient is a minimum. Liquid water accumulated in the GDL blocks gas flow and reaction sites, which results in degradation of performance and stability.

Serpentine flow channels naturally induce a pressure gradient across land areas aiding in convective transport. However, they suffer from large pressure drops due to their long flow paths, resulting in high parasitic power requirements compared to both parallel and interdigitated flow fields. This results in a large concentration gradient along the channel leading to a dry inlet and flooded outlet [1,2]. Interdigitated designs force all gases to undergo cross flow through the GDL to increase convective transport under land areas. As a result they have a high pressure drop across the cell (compared to parallel flow fields) and channel flooding issues [2,3]. Our hypothesis is that creating parallel channels with differential pressures will force the water from the high pressure channels (HPCs) under the lands into the low pressure channels (LPCs), aiding in water removal, while minimizing the distance and pressure drop between the inlet and outlet (Fig. 1). Secondly, the pressure gradient could aid in mass transport problems by bringing additional oxygen through the GDL to the CL via convection. By increasing the amount of water being removed and oxygen being delivered to the CL we can increase performance over a range of operating conditions.

Reactant flow over the lands, i.e. cross flow [4–10], has been heavily investigated in PEM fuel cells with serpentine flow fields. Pharoah utilized computational methods to determine that convective transport in the GDL is significant in serpentine flow channels [4]. Kanezaki et al. numerically investigated cross flow in a single serpentine channel and partially attributed the additional liquid water removal to the good performance of serpentine channels [5]. Park and Li studied cross flow experimentally and numerically and

* Corresponding author. Tel.: +1 530 752 5559; fax: +1 530 752 4158.
E-mail address: jwpark@ucdavis.edu (J.W. Park).

0378-7753/$ – see front matter © 2011 Elsevier B.V. All rights reserved.
doi:10.1016/j.jpowsour.2011.09.047

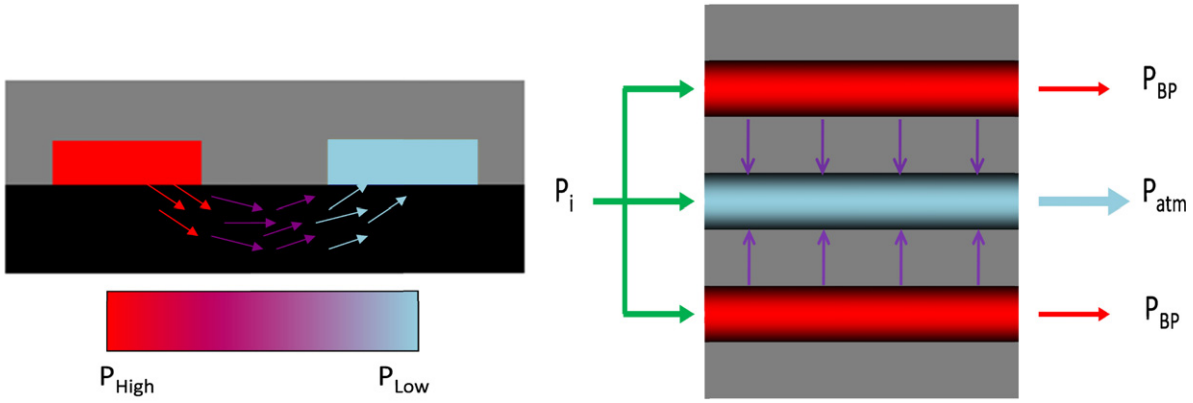

Fig. 1. Illustrations of parallel flow field with induced cross flow design. *Left*: Cross-section of flow channels, with the black layer being the GDL, the gray being the flow channel plate, the red channel being the HPC, the blue channel being the LPC, and the arrows depict the induced cross flow between channels. *Right*: Through-plane view of the three center channels of flow channel plate. P_i is the pressure at the inlet, P_{BP} is the higher back pressure supplied to the HPC exits, and P_{atm} is the atmospheric pressure at the LPC exits. (For interpretation of the references to color in this figure legend, the reader is referred to the web version of the article.)

showed that it not only aided in water removal, but considerably lowered the overall pressure drop across the cell as permeability and thickness of the GDL were increased [6]. Park and Li later established an analytical method for determining the pressure drop and average volume flow rate of cross flow in serpentine flow channels [7]. Oosthuizen et al. numerically studied the conditions where cross flow effects the pressure and temperature distribution within a serpentine channel [8]. Shi and Wang used a 3D numerical model solved with COMSOL Multiphysics to study the effect of GDL deformation on cross flow in a serpentine flow field [9]. Serpentine flow channels have even been designed to maximize cross flow by Suresh et al. and strong improvements in performance have been found with computational fluid dynamics analysis and experimental analysis [10].

Additionally, there have been many studies on flow through the GDL. Litster et al. used a fluorescence microscopy technique to visualize liquid water transport through the GDL and concluded that transport is dominated by fingering and channeling [11]. Jiao et al. visualized liquid water transport by using transparent flow channels and confirmed that cross flow is effective at removing water under the land areas [12]. Park et al. compared these experimental results with a numerical model utilizing impermeable random cylinders and found good agreement with experimental results [13]. Benziger et al. looked at water flow through carbon paper and carbon cloth GDLs and found that a minimum pressure was required to overcome the surface energy of the water and Teflon interface in large pores and found that the smaller pores remained free of water to permit gases to reach the CL [14]. Gostick et al. found in-plane and through-plane gas permeability of common GDL materials at different compressions. Further, they found materials to be significantly anisotopic with permeabilities varying by a factor of 2 in different directions [15]. Similarly, the flow in the cathode CL has also been studied analytically by Das et al. Das et al. concluded that the wetting of the cathode CL significantly affects liquid water transport and cell performance [16].

Parallel flow channels and general flow channel design have been carried out. Li et al. suggested a design procedure for serpentine channels based on establishing a pressure drop that absorbs and removes all liquid water from the cell. However, their design technique is easily applied to parallel flow channels and their design principles are useful in all flow channel patterns [1]. Li and Sabir also presented a broad review of flow field designs in PEM fuel cells [2]. Hamilton and Pollet also reviewed various basic flow field designs and extended their scope to convection enhanced serpentine, bio inspired, and porous channel flow fields [17]. Wang et al. used a 3D numerical model to explore the effect of channel aspect ratio in parallel and interdigitated flow fields on transport phenomena and cell performance. They found that low aspect ratios (larger width than height) and smaller cross-sectional areas improve water removal and performance of parallel flow fields [18]. Scholta et al. found that channel dimensions between 0.7 mm and 1 mm were optimal in parallel flow channels and that small dimensions are preferred for high current densities and larger dimensions are better for low current densities. Further, they found rib to channel ratios greater than one improved performance [19].

Although the cross flow has been investigated extensively in the past, no experimental result has been reported to utilize the benefit of cross flow in the PEM fuel cells with parallel flow channels. Our design attempts to gain the benefits of a pressure gradient across the lands that are attained with serpentine and interdigitated flow fields, without the high parasitic losses and large concentration gradient from inlet to outlet. Similar effects can be achieved by two separate flow or pressure controllers on the inlet of the high and low pressure channels, however the present design is intended to be simple and cheap and introduces cross flow in the parallel flow channels, which is the most common flow field design of modern PEM fuel cell stacks.

2. Experimental setup

A PEM fuel cell capable of both hybrid and parallel flow was designed and fabricated. The cell back plates are aluminum, the flow channel plates are nickel coated aluminum, and between the back plates and flow channel plates are brass electrical contacts. Flow channels are 20 cm long and have a 1 mm by 1 mm cross-section with 1 mm width lands. There are 7 channels, 4 HPCs with 3 LPCs in-between. The active area is 203 mm × 15 mm = 30.45 cm^2. An example of the fuel cell flow channel plates and a flow field schematic are displayed in Fig. 2. The cell used a SGL 10BC carbon gas diffusion layer and a Nafion 112 membrane electrode assembly with a platinum loading of 0.4 mg cm^{-2} on both sides. The cell was arranged with co-flowing anode and cathode so that gravity would aid in water removal (both outlets on the bottom). The outlets of the LPCs were vented to atmosphere, while the HPCs were connected to a chamber with a back pressure regulator.

The cell was evaluated through the use on an Arbin Instruments Fuel Cell Test Station located at University of California at Davis. Fig. 3 displays the fuel cell test station, test fuel cell, back pressure regulator, and disassembled test cell on the right and a simplified fuel cell test station schematic on the left. The fuel cell test

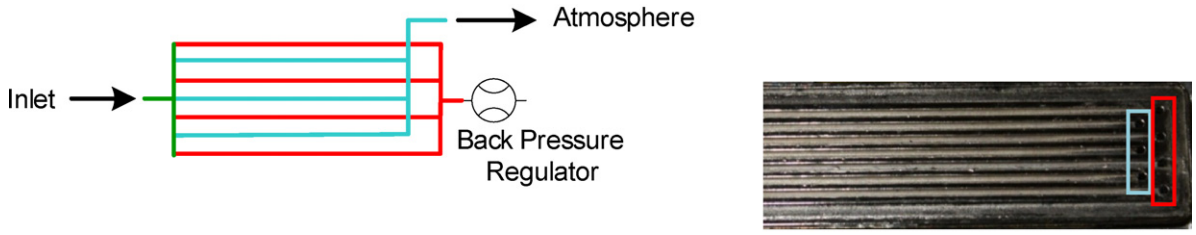

Fig. 2. *Left*: Schematic of parallel flow field with induced cross flow with one common inlet and two exit manifolds. One manifold is connected to the LPCs and is released to the atmosphere and the other manifold is connected to the HPCs and runs to the back pressure regulator. *Right*: Exit of cathode flow channel plate. The red box surrounds HPC exits and the blue box surrounds LPC exits. During the standard parallel flow, both manifolds are released to the atmosphere. (For interpretation of the references to color in this figure legend, the reader is referred to the web version of the article.)

station can measure voltage and current while easily modifying inlet conditions (temperatures, relative humidities, flow rates, etc.). Inlet and back pressure regulator pressures were measured with Miljoco low pressure gauges. The cell was operated at 80 °C with stoichiometries of 3 or 5 for air and 1.5 for hydrogen. Gas streams were heated to 80 °C and humidified to a dew point of 75 °C before entering the fuel cell. A dew point of 75 °C was chosen based on the calculated pressure drop and water creation on the cathode side in order to minimize drying and liquid water formation.

In order to measure the polarization curves, first the test cell was purged for 30 s removing bulk water from the cell, secondly the test cell, gas streams, and humidifiers were warmed-up at 0.5 V for 2 min, followed by measuring the polarization curve by stepping-up the current 1 A and holding for 30 s between steps (25 s to reach steady state and 5 s of data collection), until the voltage dropped to 50 mV. Data was collected at 1 Hz and all 5 readings at each current were averaged. Polarization curves were measured for 5 different back pressure settings. Back pressures on the HPCs were 0 (parallel), 0.7 kPa, 1.4 kPa, 1.7 kPa, and blocked for the case with a stoichiometry of 3 on the cathode. Back pressures on the HPCs were 0 (parallel), 2.4 kPa, 4.5 kPa, 5.5 kPa, and blocked for the case with a stoichiometry of 5 on the cathode. The back pressure was controlled with a back pressure regulator, however the back pressure changes slightly due to flow rate, which varies throughout the entire polarization curve. Further, the beginning of the polarization curve utilizes small flow rates and if the back pressure regulator setting is higher than the maximum attainable back pressure, the regulator setting will not be reached. For this reason, all back pressure settings during polarization curve measurements were set at 1 SLPM when using a stoichiometry of 3 on the cathode and 2 SLPM when using a stoichiometry of 5. The back pressure was set before each test and the valve setting was kept constant until the next testing condition. This was done in part because it was found that at low flow rates, which correspond to high voltages, there was minimal difference due to the back pressure settings. Thus the back pressure setting was established at a flow rate where the performance was known from previous tests to deviate based on the back pressure setting. Additionally, for the concept to be easily applied, it should be simple and inexpensive, thus a back pressure regulator was chosen rather than a feedback controlled back pressure regulator. However, after the maximum back pressure surpassed the back pressure setting, the back pressure remained reasonably constant at the back pressure setting with changes in flow rate (in general the back pressure will continue to increase with increased flow rate).

For the measurements of current density and net power at steady state voltages, the fuel cell was purged for 10 s to remove any bulk water, operated open circuit for 1 min to warm-up the gas streams and humidifier, then warmed-up the test cell at the testing voltage for 2 min before collecting data at 1 Hz for 2 min. The test fuel cell was run at 0.5 V, 0.3 V, and 0.1 V while randomizing the order of back pressure settings during each voltage run. Voltages were not randomized (there are no comparisons between different voltage conditions) to keep the cell and inlet conditions as consistent as possible for comparison between different back pressures. During the tests, stoichiometries of 3 or 5 for air and 1.5 for hydrogen were used. By utilizing constant stoichiometries the flow rate and inlet pressure changes between voltage conditions. The

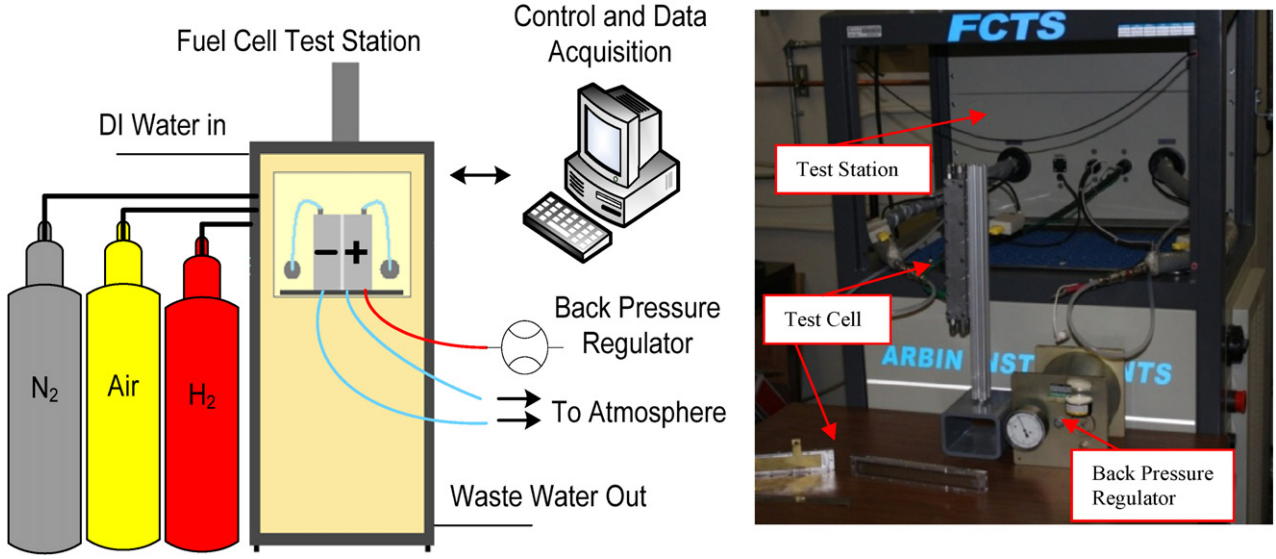

Fig. 3. *Left*: Schematic of fuel cell test station setup. *Right*: Arbin fuel cell test station, test fuel cell, back pressure regulator, and disassembled example test fuel cell.

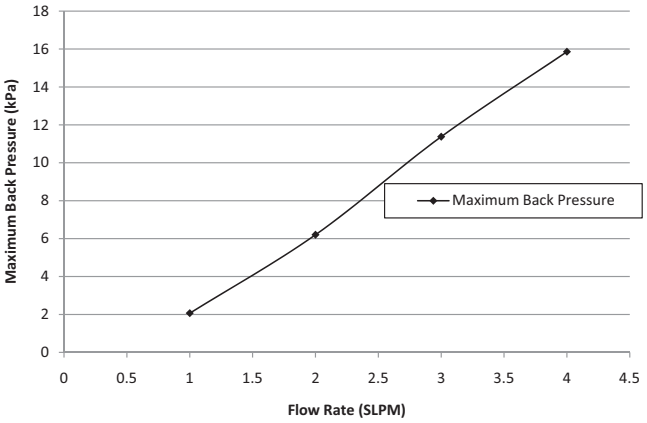

Fig. 4. Measured maximum back pressures versus flow rate.

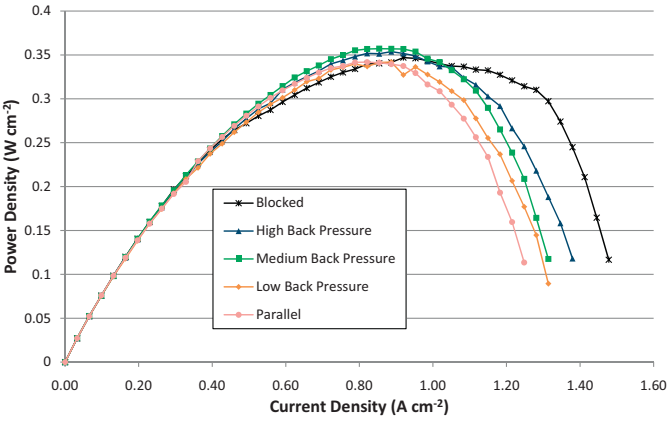

Fig. 6. Power density versus current density for a stoichiometry of 3 and varying back pressure on HPC exits.

maximum back pressure attainable is equal to the inlet pressure (measured maximum back pressures are actually slightly lower due to cross flow), therefore the range of possible back pressures is significantly different between each voltage. Due to this, we selected to run four cases for each voltage setting: standard parallel flow, low back pressure (roughly 33% of maximum back pressure), high back pressure on power channels (roughly 67% of maximum back pressure), and the final condition was blocking the HPC exits. Maximum back pressures at varying flow rates were measured by varying the flow rate through the test cell with the HPC exits connected to the closed back pressure regulator (Fig. 4).

3. Experimental results and discussion

3.1. Polarization curves

Figs. 5 and 6 show polarization and power density curves for varying back pressure on the HPC exits for a stoichiometry of 3 on the cathode. Cell voltage was found to be similar at current densities less than 0.5 A cm^{-2}, which may correspond to the activation and part of the ohmic loss region. It should be noted that the cross flow is small at low reactant flow rates and does not significantly reduce activation and ohmic losses. However, the voltage gains gradually increase as the current density increases in the range between 0.5 A cm^{-2} and 1.1 A cm^{-2} and relatively large voltage gains are found at current densities greater than 1.1 A cm^{-2} in the mass transport loss region. The voltage gains in this region may be attributed to the reactant transport through the GDL under the land area by cross flow, which is more active as the current density increases. For a stoichiometry of 3, it was found that there was an optimal back pressure between extremes that attained the highest performance. The exit of HPCs becomes blocked at the highest back pressure and as a result, the HPCs may become flooded as liquid water from the HPCs is forced to flow through the GDL to the LPCs. This might cause congestion of reactant flow in the HPCs leading to a performance decrease. Thus, the optimal back pressure should create significant amount of cross flow while not inhibiting flow through the HPCs.

Figs. 7 and 8 show polarization and power density curves for varying back pressure on the HPC exits for a stoichiometry of 5 on the cathode. Voltage gains are noticeable at current densities greater than 0.7 A cm^{-2} and are considerable at current densities greater than 1 A cm^{-2}. Further, voltage gains for a stoichiometry of 5 were found to increase with rising back pressure. Output power was also significantly increased and peak power output was shifted to higher current densities with rising back pressure, as shown in Fig. 8. This may be attributed to the inlet pressures being high enough to sustain reactant transport in the HPCs and purge the water out through the GDL, even with the HPC exits blocked.

However, a significant drop in performance was found with both stoichiometries in the blocked channel case at low flow rates, those corresponding to voltages greater 0.6 V for stoichiometry of 3 and 0.55 V for a stoichiometry of 5. We believe this is due to the inhibited

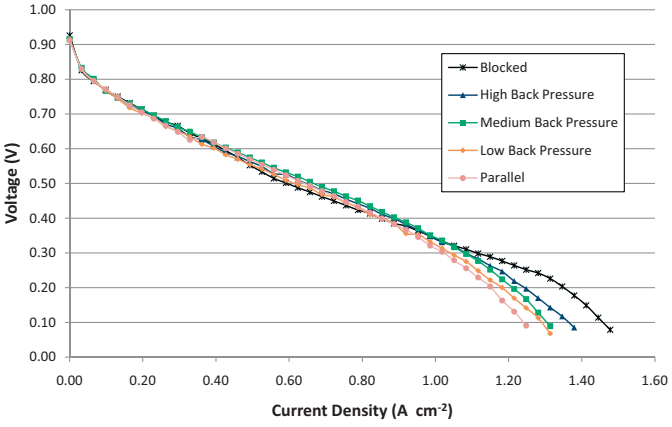

Fig. 5. Polarization curves for a stoichiometry of 3 on the cathode and varying back pressure on HPC exits. The legend goes from the setting with the highest current density, at low voltages, at top (darker) to the lowest performing at bottom (lighter).

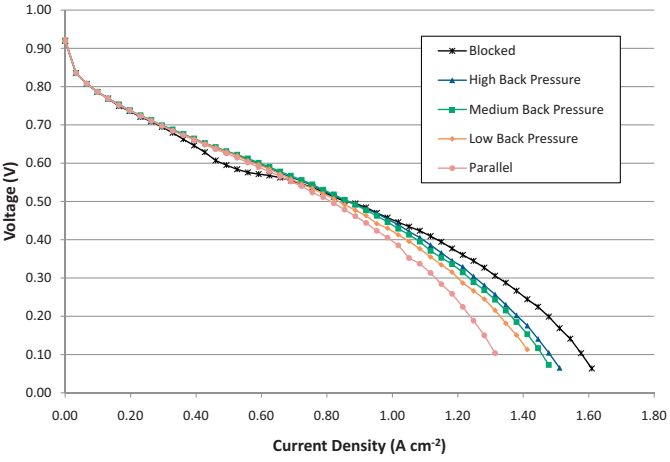

Fig. 7. Polarization curves for a stoichiometry of 5 on the cathode and varying back pressure on HPC exits. The legend goes from the setting with the highest current density at low voltages at top (darker) to the lowest performing at bottom (lighter).

Table 1
Current density and net power comparison for a stoichiometry of 3 on the cathode. Highlighted in bold are the highest values for each voltage condition.

	Stoichiometry of 3 for air and 1.5 for hydrogen											
Voltage (V)	0.5 V				0.3 V				0.1 V			
Back pressure range	Parallel	Low	High	Blocked	Parallel	Low	High	Blocked	Parallel	Low	High	Blocked
Back pressure on HPCs (kPa)	0.0	0.7	1.4		0.0	2.1	3.4		0.0	2.8	5.5	0.0
Inlet pressure (kPa)	1.4	2.2	2.6	3.4	2.8	5.2	6.2	6.9	3.6	6.9	8.6	11.7
Compressor power (W)	0.03	0.05	0.06	0.08	0.09	0.18	0.23	0.25	0.15	0.30	0.39	0.55
Average current density (A cm^{-2})	0.71	0.70	0.73	0.71	1.03	1.12	1.18	1.14	1.28	1.39	1.45	1.50
% change in current density from parallel	0.0%	−0.8%	**3.2%**	1.0%	0.0%	8.6%	**14.5%**	10.5%	0.0%	8.6%	13.3%	**17.1%**
Net power density (W cm^{-2})	0.35	0.35	0.36	0.35	0.31	0.33	0.35	0.33	0.12	0.13	0.13	0.13
% change in net power density from parallel	0.0%	−1.0%	**2.9%**	0.5%	0.0%	7.7%	**13.2%**	8.9%	0.0%	4.8%	**7.3%**	7.1%

reactant flow in the HPCs, along with inadequate removal of liquid water.

3.2. Net power enhancement

A steady state performance test has been carried out to evaluate the net power enhancement by the parallel flow field with induced cross flow. The current density of the cell during each run at constant voltage was measured every second for 2 min. All current measurements were averaged for each trial and the current densities were compared. The required compressor power was approximated by knowing the inlet pressure, mass flow rate for each run condition, and assuming a compressor isentropic efficiency of 85%.

Performance gains were found at all voltages for a stoichiometry of 3 on the cathode (Table 1). At 0.5 V a 3% gain in current density and net power were found at the optimal back pressure (back pressure resulting in the highest current density). While running at 0.3 V and 0.1 V significant gains in current density were found of 15% and 17%, respectively. When including the additional pumping work required, the net power gains at 0.3 V and 0.1 V were found to be 13% and 7%, respectively. Interestingly, both the peak current density and net power at 0.5 V and 0.3 V were found to occur while applying elevated back pressure on the HPCs and not at the most extreme cases of blocking the HPCs or during the standard parallel flow. This is evidenced that there is a favorable back pressure where maximum performance is attained. At 0.1 V the flow rate is high enough in the blocked case to purge the HPCs and thus the blocked case has the highest current density (17% increase from the parallel flow field case). However, when including the additional pumping work, which is significantly higher due to high flow rates, the net power increases were again at the high back pressure setting. Inlet pressure and back pressure setting for the optimal case are plotted versus current density for each voltage condition, with a stoichiometry of 3, in Fig. 9.

Larger gains in performance at all voltages were found for a stoichiometry of 5 on the cathode (Table 2). Conversely, net power gains were only found at 0.5 V and 0.3 V. At 0.5 V and 0.3 V a 22% and 24% gain in current density were found and an 8% and 14% gain in net power were found in the optimal case (blocked HPCs). At 0.1 V the blocked case had 24% increase in current density, but due to high pumping losses at 0.1 V, all cases had negative net power improvement. The blocked case had the highest performance in all three cases when utilizing a stoichiometry of 5 because the pressure in the HPCs is high enough to purge all liquid water and induce flow through the GDL. Inlet pressure and back pressure setting for the optimal case are plotted versus current density for each voltage condition, with a stoichiometry of 5, in Fig. 10.

Finally, to confirm that the voltage and power gains were achieved by cross flow, but not by raised average pressure in the HPCs, the cell performance was evaluated with 14 kPa of back pressure on all channels (standard parallel flow) with a stoichiometry of 5. This setting showed virtually the same increase in performance as the induced cross flow with low back pressure condition, even though the average channel back pressure was ten times higher. Further, at 0.5 V a power output improvement of only 3.5% was measured, resulting in a 1% loss in net power when subtracting pumping losses. Thus, the increase in performance in the parallel flow with induced cross flow, from an increase in operating pressure, is minimal compared to gains from cross flow.

4. Conclusion

A PEM fuel cell capable of both parallel flow and parallel flow with induced cross flow through the cathode was designed, built, and tested. Polarization curves were measured for different back

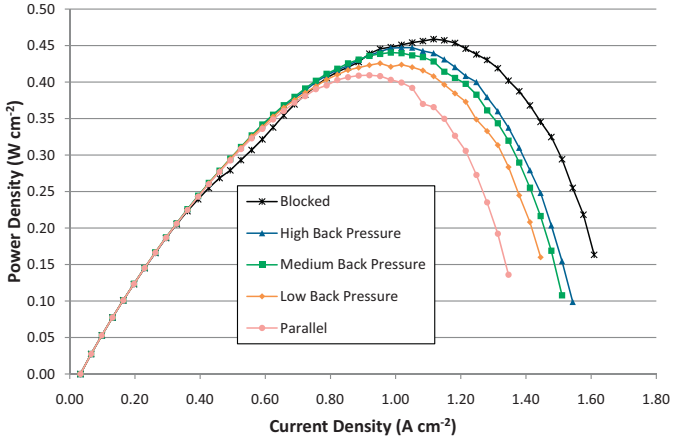

Fig. 8. Power density versus current density for a stoichiometry of 5 and varying back pressure on HPC exits.

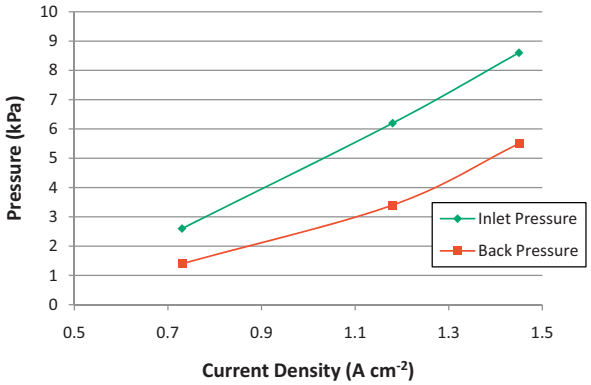

Fig. 9. Measured inlet pressure and back pressure setting versus current density for the optimal steady state conditions with a stoichiometry of 3.

Table 2
Current density and net power comparison for a stoichiometry of 5 on the cathode. Highlighted in bold are the highest values for each voltage condition.

	Stoichiometry of 5 for air and 1.5 for hydrogen											
Voltage (V)	0.5 V				0.3 V				0.1 V			
Back pressure range	Parallel	Low	High	Blocked	Parallel	Low	High	Blocked	Parallel	Low	High	Blocked
Back pressure on HPCs (kPa)	0.0	2.4	4.5		0.0	4.5	8.3		0.0	6.6	12.8	
Inlet pressure (kPa)	7.0	9.0	10.0	12.0	9.0	14.0	17.0	21.0	11.0	18.0	21.0	27.0
Compressor power (W)	0.31	0.42	0.46	0.57	0.55	0.93	1.16	1.50	0.77	1.39	1.75	2.23
Average current density ($A\,cm^{-2}$)	0.84	0.90	0.89	0.92	1.16	1.29	1.34	1.42	1.35	1.52	1.66	1.67
% change in current density from parallel	0.0%	6.7%	5.8%	**9.6%**	0.0%	11.0%	15.0%	**22.0%**	0.0%	12.8%	22.7%	**23.9%**
Net power density ($W\,cm^{-2}$)	0.41	0.44	0.43	0.44	0.33	0.36	0.36	0.38	0.11	0.11	0.11	0.09
% change in net power density from parallel	0.0%	5.9%	4.7%	**7.7%**	0.0%	7.8%	9.8%	**13.8%**	**0.0%**	−2.8%	−1.4%	−14.4%

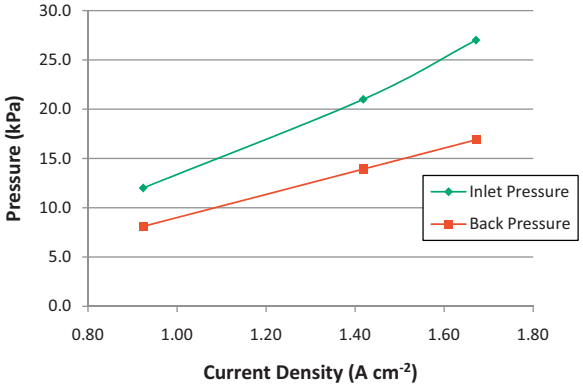

Fig. 10. Measured inlet pressure and back pressure setting versus current density for the optimal steady state conditions with a stoichiometry of 5.

pressures on the HPCs and for different stoichiometries on the cathode. Performance gains from induced cross flow were found at voltages less than 0.55 V. When using a stoichiometry of 3 on the cathode, the elevated back pressure settings were the highest performing except at voltages less than 0.3 V, where the blocked case was able to purge the HPCs. When utilizing a stoichiometry of 5, the blocked case was the highest performing for voltages less than 0.5 V as the flow rates are high enough to purge the HPCs. The largest differences in performance were found at the end of the ohmic and mass transport loss region. Constant voltage testing was done at 0.5 V, 0.3 V, and 0.1 V for different back pressures applied to the HPCs and for different stoichiometries on the cathode. Gains in current density were found at 0.5 V, 0.3 V, and 0.1 V of up to 3%, 15%, and 17%, respectively for a stoichiometry of 3 on the cathode and 10%, 22%, and 24%, respectively for a stoichiometry of 5. Further, gains in net power when subtracting approximated pumping losses were found at 0.5, 0.3 V, and 0.1 V of 3%, 13%, and 7%, respectively for a stoichiometry of 3 and 8%, 14%, and −1% for a stoichiometry of 5. Peak gains in net power were found between extreme cases of 0 back pressure (standard parallel flow) and blocking the HPC exits at lower flow rates (those corresponding to current densities less than $0.9\,A\,cm^{-2}$). This suggests that there is a critical back pressure that does not block the HPC flow, but forces flow to cross over the lands while minimizing pumping work. By optimizing channel geometry or implementing differential pressures across the lands from inlet to the outlet, it may be possible to push performance gains into higher and more practical voltages. However, it is evident that by increasing the back pressure on the HPCs, that mass transport losses can be diminished.

References

[1] X. Li, I. Sabir, J. Park, Journal of Power Sources 163 (2007) 933–942.
[2] X. Li, I. Sabir, International Journal of Hydrogen Energy 30 (2005) 359–371.
[3] D. Spernjak, A. Prasad, S. Advani, Journal of Power Sources 195 (2010) 3553–3568.
[4] J.G. Pharoah, Journal of Power Sources 144 (2005) 77–82.
[5] T. Kanezaki, X. Li, J.J. Baschuk, Journal of Power Sources 162 (2006) 415–425.
[6] J. Park, X. Li, Journal of Power Sources 163 (2007) 853–863.
[7] J. Park, X. Li, International Journal of Energy Research 35 (2011) 583–593.
[8] P.H. Oosthuizen, L. Sun, K.B. McAuley, Applied Thermal Engineering 25 (2005) 1083–1096.
[9] Z. Shi, X. Wang, Journal of Power Sources 185 (2008) 985–992.
[10] P.V. Suresh, S. Jayanti, A.P. Deshpande, P. Haridoss, International Journal of Hydrogen Energy 36 (2011) 6067–6072.
[11] S. Litster, D. Sinton, N. Djilali, Journal of Power Sources 154 (2006) 95–105.
[12] K. Jiao, J. Park, X. Li, Applied Energy 87 (2010) 2270–2777.
[13] J. Park, K. Jiao, X. Li, Applied Energy 87 (2010) 2180–2186.
[14] J. Benziger, J. Nehlsen, D. Blackwell, T. Brennan, J. Itescu, Journal of Membrane Science 261 (2005) 98–106.
[15] J. Gostick, M. Fowler, M. Pritzker, M. Ioannidis, L. Behra, Journal of Power Sources 162 (2006) 228–238.
[16] P. Das, X. Li, Z. Liu, International Journal of Hydrogen Energy 35 (2010) 2403–2416.
[17] P.J. Hamilton, B.J. Pollet, Fuel Cells 10 (4) (2010) 489–509.
[18] X. Wang, Y. Duan, W. Yan, X. Peng, Electrochimica Acta 53 (2008) 5334–5343.
[19] J. Scholta, G. Escher, W. Zhang, L. Kuppers, L. Jorissen, W. Lehnert, Journal of Power Sources 155 (2006) 66–71.